Inorganic Chemistry

Article

pubs.acs.org/IC

Nanosized $\{Pd_4(\mu_4\text{-}C)\}Pd_{32}(CO)_{28}(PMe_3)_{14}$ Containing Tetrahedrally Deformed Pd_4 Cage with Encapsulated Carbide Atom: Formal Substitution of Geometrically Analogous Interior Au_4 Entity in Isostructural $Au_4Pd_{32}(CO)_{28}(PMe_3)_{14}$ by Electronically Equivalent $Pd_4(\mu_4\text{-}C)$ and Computational/Catalytic Implications

Evgueni G. Mednikov,*[,†] Sergei A. Ivanov,[‡] and Lawrence F. Dahl*[,†]

[†]Department of Chemistry, University of Wisconsin-Madison, Madison, Wisconsin 53706, United States

[‡]Center for Integrated Nanotechnologies, Los Alamos National Laboratory, Los Alamos, New Mexico 87545, United States

Supporting Information

ABSTRACT: This first homopalladium carbido cluster, $\{Pd_4(\mu_4\text{-}C)\}Pd_{32}(CO)_{28}(PMe_3)_{14}$ (**1**), was isolated (3−7% yields) from an ultimately simplified procedure—the reaction of $CHCl_3$ under N_2 with either $Pd_8(CO)_8(PMe_3)_7$ or $Pd_{10}(CO)_{12}(PMe_3)_6$ at room temperature. Charge-coupled device (CCD) X-ray diffraction data at 100 K for **1**·2.5 C_6H_{14} (**1a**) and **1**·3 $CHCl_3$ (**1b**) produced closely related molecular parameters for **1**. This $\{Pd_4C\}Pd_{32}$ cluster (**1**) possesses a highly unusual tetracoordinated carbide atom that causes a major distortion of a central regular Pd_4 tetrahedron into a new symmetry type of encapsulated Pd_4 cage of pseudo-D_2 (222) symmetry. Mean Pd−Pd distances for the three pairs of opposite twofold-equivalent Pd−Pd tetrahedral-like edges for **1a** are 2.71, 2.96, and 3.59 Å; the mean of the four Pd−C distances [range, 1.87(2)−1.94(2) Å] is 1.91 Å. An astonishing molecular feature is that this $\{Pd_4C\}Pd_{32}$ cluster (**1**) is an isostructural and electronically equivalent analogue of the nanosized $Au_4Pd_{32}(CO)_{28}(PMe_3)_{14}$ (**2**). Cluster **2**, likewise a pseudo-D_2 molecule, contains a geometrically analogous tetrahedrally deformed interior Au_4 entity encapsulated within an identical $Pd_{32}(CO)_{28}(PMe_3)_{14}$ shell; mean distances for the three corresponding symmetry-equivalent pairs of slightly smaller opposite tetrahedral-distorted Au−Au edges are 2.64, 2.90, and 3.51 Å. A computational study by both a natural population analysis (NPA) and an atoms-in-molecules (AIM) method performed on model analogues $\{Pd_4C\}Pd_{32}(CO)_{28}(PH_3)_{14}$ (**1-mod**) and $Au_4Pd_{32}(CO)_{28}(PH_3)_{14}$ (**2-mod**) suggested that the negatively charged Au_4 entity in **2-mod** may be described as two weakly interacting electron-pair Au_2 intradimers. In contrast, an NPA of the $\{Pd_4C\}$ entity in **1-mod** revealed that two similarly oriented identical Pd_2 intradimers of 2.71 Å are primarily stabilized by Pd−C bonding with a negatively charged carbide atom. The isostructural stabilizations of **1** and **2** are then attributed to the similar sizes, shapes, and overall negative charge distributions of the electronically equivalent interior $\{Pd_4C\}$ and Au_4 entities. This resulting remarkable structural/electronic equivalency between **1** and **2** is consistent with the greatly improved performances of commercial palladium catalysts for vinyl acetate synthesis by gold-atom incorporation to suppress carbonization of the Pd atoms, namely, that the extra Au $6s^1$ valence electron of each added Au atom provides an effective "negative charge protection" against electron-donating carbon atoms forming Pd carbido species such as $\{Pd_4C\}$.

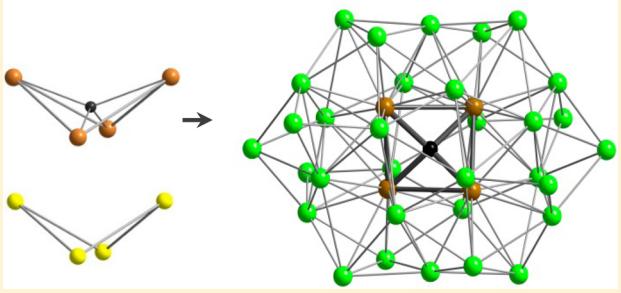

INTRODUCTION

Since the initial structural discovery in 1962 of the pentacoordinated square-pyramidal carbido atom in $Fe_5(\mu_5\text{-}C)(CO)_{15}$[1], which showed that discrete transition metal carbonyl clusters can incorporate an interstitial carbon atom, many examples of such clusters have been reported.[2] Hence, the resulting metal carbido cluster chemistry has five decades of history but continues to attract considerable attention.[3] The interest is at least twofold. First, these compounds have given rise to greatly expanded synthetic routes that have produced highly diverse transition metal clusters. Carbide atoms not only electronically stabilize (each by donation of four valence electrons) the metal cores but also allow heterometallic atom-for-atom substitution either with retention of the original metal framework or with controllable geometrical transformations.[2c,e] Second, transition metal carbide clusters are valuable models for studies of reactivity patterns of carbon atoms toward C−H and C−C bond formation as well as related C−H bond activation. In fact, their positive relevance to both stoichiometric[4] and catalytic reactions[5] primarily involving C_1 chemistry has been widely recognized. However, catalyst

Received: January 28, 2015

DOI: 10.1021/acs.inorgchem.5b00208
Inorg. Chem. XXXX, XXX, XXX−XXX

carbidization may play a highly negative role. One such example is the catalytic oxidation of ethylene into vinyl acetate (VA) in the presence of acetic acid on a supported Pd catalyst;[6a] its carbidization resulted in a marked decrease of catalytic reactivity, whereas addition of Au suppressed carbide formation and kept the catalyst active.[6b−f] Combined experimental/computational results described herein shed light on the probable origin of such a phenomenon.

Herein we present the preparation of the first homopalladium carbido cluster, $\{Pd_4(\mu_4\text{-}C)\}Pd_{32}(CO)_{28}(PMe_3)_{14}$ (**1**) by an ultimately simplified room-temperature reaction of $CHCl_3$ with either $Pd_8(CO)_8(PMe_3)_7$ or $Pd_{10}(CO)_{12}(PMe_3)_6$ precursors under N_2 together with its low-temperature X-ray crystallographic characterization of two different solvated crystalline forms. Of prime significance is that **1** provides an unprecedented example of a molecular cluster with a tetracoordinated carbon atom that is encapsulated within a new symmetry-type of tetrahedral-deformed M_4 cage to accommodate the C atom. Especially surprising is that **1** may be formally derived from the previously reported isostructural Au−Pd $Au_4Pd_{32}(CO)_{28}(PMe_3)_{14}$ (**2**)[7a] by the electronically equivalent replacement of the internal Au_4 entity in **2** with the geometrically analogous interior $\{Pd_4C\}$ entity in **1**. A detailed stereochemical/bonding comparison of **1** and **2** including natural population analyses based upon density functional theory (DFT) calculations was performed; resulting computational/catalytic implications are discussed and related to the highly preferable utilization of commercial Au−Pd catalysts (vs corresponding Pd catalysts) used in the production of VA that greatly increased reactivities and suppressed palladium carbidization.

RESULTS AND DISCUSSION

Synthesis of $\{Pd_4(\mu_4\text{-}C)\}Pd_{32}(CO)_{28}(PMe_3)_{14}$ (1). This research stems from our ongoing systematic attempts to find general synthetic pathways to obtain nanosized bimetallic Pd−Pt clusters via an exploration of the chemistry of the two separate families of CO/PR_3-ligated zerovalent Pd(0) and Pt(0) compounds. One exceptional outcome of this investigation led to isolation of the extraordinary Pt-centered icosahedral four-shell 165-atom Pd−Pt cluster of pseudo-I_h symmetry, $(\mu_{12}\text{-}Pt)Pd_{164-x}Pt_x(CO)_{72}(PPh_3)_{20}$ ($x \approx 7$), from the reaction of $Pd_{10}(CO)_{12}(PPh_3)_6$ with zerovalent $Pt(CO)_2(PPh_3)_2$.[7b] Herein we report the preparation of the carbido cluster, $\{Pd_4(\mu_4\text{-}C)\}Pd_{32}(CO)_{28}(PMe_3)_{14}$ (**1**), via a synthesis based upon our initial (unreported) preparation of the analogous Pd−Pt carbido derivative, $\{Pd_4(\mu_4\text{-}C)\}Pd_{31.2}Pt_{0.8}(CO)_{28}(PMe_3)_{14}$ (**3**). This latter cluster (**3**) was obtained from a procedure designed for the synthesis of the heterometallic Pd−Pt cluster, $Pd_{16-x}Pt_x(CO)_{13}(PMe_3)_9$ (**4**), namely, the substituted Pt-for-Pd analogue of the $Pd_{16}(CO)_{13}(PMe_3)_9$,[8] which consists of a centered icosahedral Pd_{13} architecture with three exopolyhedral wingtip Pd atoms. This procedure, which is conceptually similar to that used for the isolation of the concentric spheroidal-shaped multishell 165-atom Pd−Pt cluster $(\mu_{12}\text{-}Pt)Pd_{164-x}Pt_x(CO)_{72}(PPh_3)_{20}$ ($x \approx 7$),[7b] involved several consecutive steps: (a) formation of the PMe_3-containing butterfly Pd_4 cluster, $Pd_4(CO)_5(PMe_3)_4$, in situ from the reaction of $Pd_{10}(CO)_{12}(PMe_3)_6$ and PMe_3; (b) preparation of the corresponding mixed PMe_3-containing Pd_xPt_{4-x} butterfly cluster, also in situ, from the reaction between the isostructural homonuclear $Pd_4(CO)_5(PMe_3)_4$ and $Pt_4(CO)_5(PMe_3)_4$ in an analogous fashion to that found for the preparation of the PEt_3-containing $Pd_xPt_y(CO)_5(PEt_3)_4$, $x + y = 4$;[9] and (c) generation of $Pd_{16-x}Pt_x(CO)_{13}(PMe_3)_9$ (**4**) in accordance with the synthetic methodology developed for the preparation of the homonuclear PEt_3-containing $Pd_{16}(CO)_{13}(PEt_3)_9$ from the reaction of $Pd_4(CO)_5(PEt_3)_4$ and $HOAc/Me_3NO$.[10] In contrast to the latter reaction, which gave crystalline $Pd_{16}(CO)_{13}(PEt_3)_9$ with a high yield (>60%),[10] step (c) instead afforded a red precipitate as the main product, even though the target **4** was also observed as a minor byproduct. This red precipitate was found to be insoluble in common nonchlorinated organic solvents. Its crystallization under N_2 from $CHCl_3$/hexane vapor diffusion unexpectedly gave the crystallographically characterized bimetallic Pd−Pt carbido cluster $\{Pd_4(\mu_4\text{-}C)\}Pd_{31.2}Pt_{0.8}(CO)_{28}(PMe_3)_{14}$ (**3**) as a mixed solvate $\mathbf{3}\cdot 0.5C_6H_{14}\cdot 0.5CHCl_3$ (**3a**). Further investigation showed that formation of this black carbide cluster does not necessitate the presence of the $Pt_4(CO)_5(PMe_3)_4$ precursor and that the red precipitate is primarily composed of the $Pd_8(CO)_8(PMe_3)_7$ cluster.[11] These observations resulted in an ultimately simplified procedure for the preparation of crystalline $\{Pd_4(\mu_4\text{-}C)\}Pd_{32}(CO)_{28}(PMe_3)_{14}$ (**1**), namely, its direct isolation from reactions of $CHCl_3$ with either the PMe_3-ligated Pd_8 or Pd_{10} cluster under N_2 and concomitant/subsequent crystallizations under N_2 from $CHCl_3$ solutions in the presence of hexane. Yields (3−7%) of **1**, somewhat better with the Pd_8 precursor, are kinetically controlled and mainly affected by the time (an optimum of 1−3 d) of keeping $CHCl_3$ solutions prior to contact with hexane vapor. If crystallization was set up immediately after dissolution of the Pd_8 cluster in $CHCl_3$, it gave a mixture of crystalline **1** together with square-planar $PdCl_2(PMe_3)_2$ (**5**) and the red precursor $Pd_8(CO)_8(PMe_3)_7$. On the contrary, too long storage (up to 10 d) of an initially dark red (and then dark brown) solution of the Pd_8 precursor in $CHCl_3$ led to its complete color fading due to in situ decomposition of **1**, accompanied by precipitation of Pd black and formation of colorless **5**. The halocarbon $CHCl_3$ was previously shown by Chini and co-workers[12] to be the source of the carbide atom in their preparation of the trigonal prismatic $[Rh_6(\mu_6\text{-}C)(CO)_{15}]^{2-}$ dianion. Our change from $CHCl_3$ to the perchlorinated reagent hexachloropropene C_3Cl_6, which was utilized[13] for generation of the size-comparable Ni_{38} polycarbido cluster anion $[Ni_{38}C_6(CO)_{42}]^{6-}$, did not afford **1** or any other crystalline products.

There is no doubt that the initial driving force toward the formation of **1** is an oxidative addition of $CHCl_3$ to the CO/PMe_3-ligated Pd(0) species. The resulting most stable product of such a reaction is the Pd(II) complex (**5**), $PdCl_2(PMe_3)_2$, which is always observed upon completion of the reaction of either the Pd_8 or Pd_{10} precursor with chloroform. Furthermore, the $Pd_4(\mu_3\text{-}CH)(\mu\text{-}Cl)_3(P^tBu_3)_4$ cluster with a μ_3-methylidyne ligand was previously isolated by Mingos and co-workers[14] from the reaction of $CHCl_3$ with a Pd(0) species. This tetrapalladium cluster, even with the absence of the "pure" carbide atom and with its resulting small metal-core size compared to that of **1**, is nevertheless especially relevant to **1**. First, its simple synthesis involving reaction of $Pd_2dba_3\cdot C_6H_6$ (dba = dibenzylideneacetone) with P^tBu_3 followed by addition of $CHCl_3$[14] is conceptually identical to the preparation of **1**. In fact, the bulky P^tBu_3 ligands and the absence of carbon monoxide are presumably responsible for its formation; otherwise, in the presence of CO and with PMe_3 (instead of P^tBu_3) either the same precursor $Pd_8(CO)_8(PMe_3)_7$[11] used to synthesize **1** or an analogous one would be generated. Second,

DOI: 10.1021/acs.inorgchem.5b00208
Inorg. Chem. XXXX, XXX, XXX−XXX

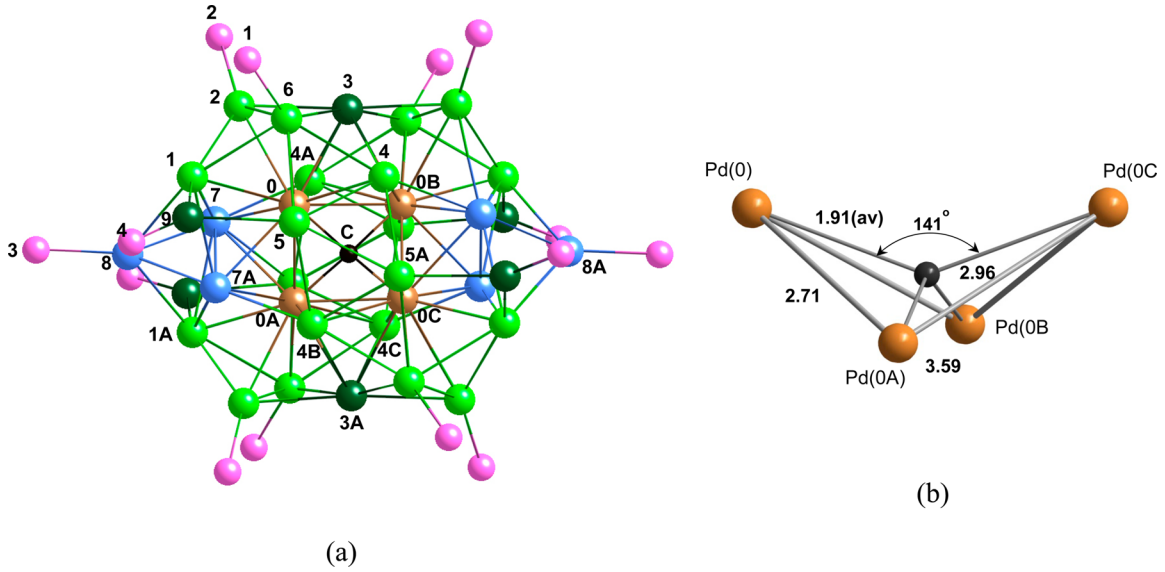

Figure 1. (a) Side view of the molecular structure (with atom-labeling) of homopalladium carbido $\{Pd_4(\mu_4\text{-}C)\}Pd_{32}P_{14}$ cluster (**1**) of pseudo-D_2 symmetry (without P-attached Me substituents and 28 bridging COs) oriented with in-plane horizontal and vertical C_2 axes and the third out-of-plane C_2 axis each intersecting the central carbido atom and passing through the midpoints of the pair of opposite twofold-equivalent Pd−Pd edges. (b) Interior $\{Pd_4(\mu_4\text{-}C)\}$ entity of **1** containing a new symmetry type of encapsulated tetrahedral-deformed Pd_4 cage (accommodating the tetracoordinated carbide atom) of pseudo-D_2 geometry with three pairs of opposite twofold-equivalent tetrahedral-like Pd−Pd edges being 2.71 (average (av)), 2.96 (av), and 3.59 (av) Å for solvated **1**·2.5 C_6H_{14} (**1a**); the mean of the four Pd−C distances (range, 1.87(2)−1.94(2) Å) is 1.91 Å.

Table 1. Mean Distances (Å) and Corresponding Individual Ranges (Å) under Pseudo-D_2 Symmetry for Central $Pd_4(\mu_4\text{-}C)$ Entity of $\{Pd_4(\mu_4\text{-}C)\}Pd_{32}(CO)_{28}(PMe_3)_{14}$ (1) in Solvated 1·2.5 C_6H_{14} (1a) and 1·3 $CHCl_3$ (1b)

entry	connectivity[a]	N[b]	1a		1b	
1	Pd-(μ_4-C)	4	1.91	1.87(2)−1.94(2)	1.91	1.88(2)−1.94(2)
2	Pd(0)−Pd(0A)[c]	2	2.71	2.706(2), 2.706(2)	2.71	2.707(2), 2.707(2)
3	Pd(0)−Pd(0B)[d]	2	2.96	2.954(2), 2.970(2)	2.99	2.976(2), 2.999(2)
4	Pd(0)···Pd(0C)[e]	2	3.59	3.572(2), 3.614(2)	3.60	3.597(2), 3.599(2)

[a]Atom-labeling for the four equivalent carbide-connected Pd(0), Pd(0A), Pd(0B), Pd(0C) atoms is shown in Figure 1. [b]N denotes number of symmetry-equivalent atom-pair connectivities under pseudo-D_2 symmetry. [c]Equivalent atom-pair is Pd(0B)−Pd(0C). [d]Equivalent atom-pair is Pd(0A)−Pd(0C). [e]Equivalent atom-pair is Pd(0A)−Pd(0B).

this tetrapalladium $Pd_4(\mu_3\text{-}CH)(\mu\text{-}Cl)_3(P^tBu_3)_4$ compound formally contains all of the elemental components of the $CHCl_3$ molecule including the μ_3-CH group and thereby provides a prototype for unobserved intermediates in our reactions of either the Pd_8 or Pd_{10} precursor with $CHCl_3$ that gave rise to **1**. This suggestion is also based on known examples of the facile conversion of μ_3-CH groups into carbido species.[15] In the synthesis of **1**, reductive elimination of HCl via dissociation of a possible μ_3-methylidyne intermediate would be facilitated by its coordination with stoichiometrically available basic PMe_3 to form a phosphonium salt, $[HPMe_3]Cl$. Thus, the reaction leading to **1** most likely occurs via consecutive oxidative addition and reductive elimination processes with presumed products that may be formulated as follows:

$$Pd_8(CO)_8(PMe_3)_7 \text{ or } Pd_{10}(CO)_{12}(PMe_3)_6 + CHCl_3 \rightarrow [Pd_n(\mu_3\text{-}CH)Cl_x(CO)_y(PMe_3)_z] \text{ [possible intermediate(s)]} \rightarrow \mathbf{1} + Pd_{black} + PdCl_2(PMe_3)_2 + [HPMe_3]Cl \quad (1)$$

During our investigation of possible pathways toward bimetallic Pd−Pt clusters we also obtained and crystallographically characterized $Pd_{12.7}Pt_{3.3}(CO)_{13}(PMe_3)_9$ (**4**) as the solvated **4**·0.5$(CH_3)_2CO$·0.3C_4H_8O (**4a**), together with the butterfly tetraplatinum $Pt_4(CO)_5(PMe_3)_4$. Crystal structures of heterometallic **4** and earlier mentioned **3** will be published elsewhere along with crystal structures of other Pd/Pt clusters that we have isolated.

Solid-State Structure of $\{Pd_4(\mu_4\text{-}C)\}Pd_{32}(CO)_{28}(PMe_3)_{14}$ (1) and Its Stereochemical/Electronic Equivalence to $Au_4Pd_{32}(CO)_{28}(PMe_3)_{14}$ (2). *(a) General Comments.* The molecular structure of **1** was obtained from complete charge-coupled device (CCD) X-ray diffractometry determinations at 100 K of two isolated solvated crystalline forms, namely, **1**·2.5C_6H_{14} (**1a**) and **1**·3$CHCl_3$ (**1b**), each of which crystallizes in a triclinic unit cell (with $Z = 2$) under centrosymmetric $P\bar{1}$ symmetry such that one molecule of **1** is crystallographically independent. Figure 1 shows the geometry of the $\{Pd_4(\mu_4\text{-}C)\}Pd_{32}P_{14}$ fragment of **1** (without the 28 CO ligands and P-attached Me substituents) together with its unprecedented interstitial interior $Pd(i)_4$ cage that contains the carbide atom. Table 1 presents the mean distances and ranges under pseudo-D_2 symmetry for the central $Pd_4(\mu_4\text{-}C)$ entity in **1a** and **1b**. Figure 2 presents comparative views of the entire molecular geometries of the isostructural $\{Pd_4(\mu_4\text{-}C)\}Pd_{32}$ **1** and Au_4Pd_{32} **2** (without the P-attached methyl substituents). Figure 3 displays the proposed formal generation of the $\{Pd_4(\mu_4\text{-}C)\}Pd_{32}P_{14}$ framework of **1**, which parallels that given in Figure

DOI: 10.1021/acs.inorgchem.5b00208
Inorg. Chem. XXXX, XXX, XXX−XXX

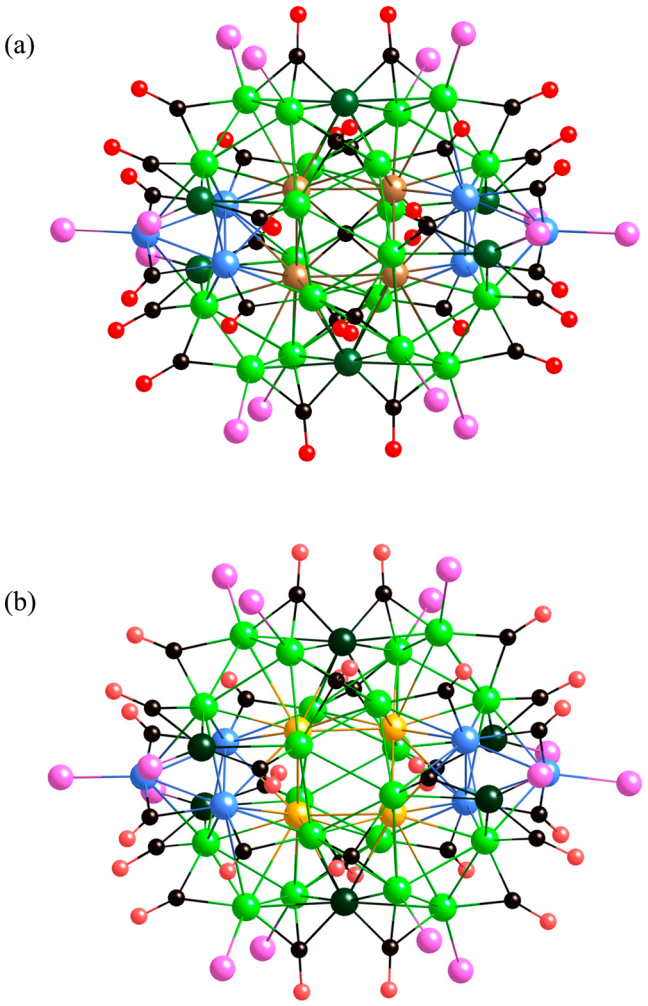

Figure 2. Comparison of closely related molecular structures (without phosphine-attached Me substituents) of (a) $\{Pd_4(\mu_4\text{-}C)\}Pd_{32}(CO)_{28}(PMe_3)_{14}$ (**1**) from crystal-solvated **1**·2.5 C_6H_{14} (**1a**); and of (b) $Au_4Pd_{32}(CO)_{28}(PMe_3)_{14}$ (**2**) from crystal-solvated **2**·3THF·Et_2O (**2a**). Both isostructural molecules **1** and **2** are displayed in virtually identical orientations (as in Figure 1) to highlight their remarkably analogous ligations. The coloring scheme is the same as in Figure 1; the Au atoms are shown in light yellow. The isostructural stabilizations of **1** and **2** are presumed to be a consequence of the similar sizes, shapes, and overall negative charge distributions of the electronically equivalent interior C-filled Pd_4 and empty Au_4 cages, respectively, supported by encapsulations within identical $Pd_{32}(CO)_{28}(PMe_3)_{14}$ shells.

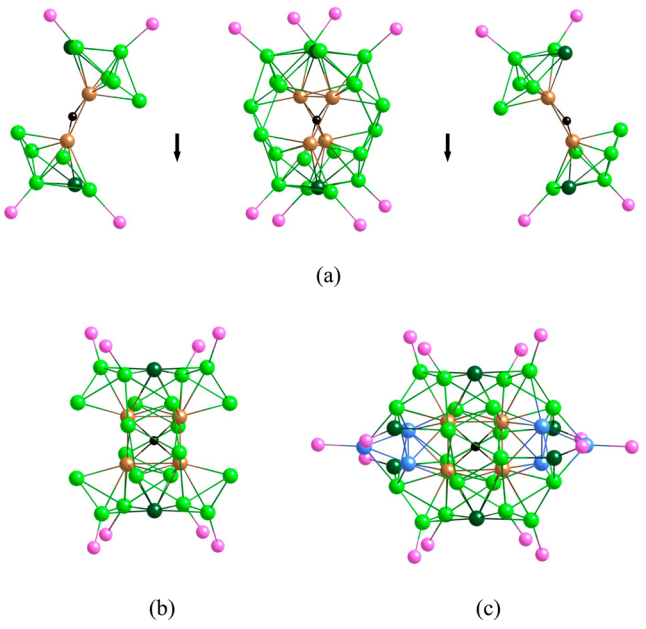

Figure 3. Anatomy showing proposed buildup of icosahedral $\{Pd_4(\mu_4\text{-}C)\}Pd_{32}P_{14}$ framework of **1** from the following: (a) Formation of twinned composite $\{Pd_4(\mu_4\text{-}C)\}Pd_{22}P_8$ kernel (center) from interpenetration of two identical "open" bis(pentagonal-bipyramidal) $\{Pd_2(\mu_4\text{-}C)\}Pd_{12}P_4$ intradimers (left and right) via vertex-fusion of carbide atom (black) and two Pd atoms (dark green). (b) Another view of $\{Pd_4(\mu_4\text{-}C)\}Pd_{22}P_8$ kernel after 90° rotation about in-plane vertical pseudo-C_2 axis passing through carbide and two dark green Pd atoms. (c) Entire $\{Pd_4(\mu_4\text{-}C)\}Pd_{32}P_{14}$ fragment of **1** formed by addition of six blue-colored Pd atoms (with two horizontally attached P atoms) and four exopolyhedral edge-bridged dark green Pd atoms, each with an attached P atom.

4 for the previously proposed analogous formation of the corresponding $Au_4Pd_{32}P_{14}$ framework of **2**.[7a] Table S1 (Supporting Information) presents a comparison of corresponding mean distances and ranges of individual distances under pseudo-D_2 molecular symmetry for $\{Pd_4(\mu_4\text{-}C)\}Pd_{32}(CO)_{28}(PMe_3)_{14}$ (**1**) in **1**·2.5C_6H_{14} (**1a**) and **1**·3$CHCl_3$ (**1b**) together with the isostructural $Au_4Pd_{32}(CO)_{28}(PMe_3)_{14}$ (**2**) in **2**·3THF·Et_2O (**2a**; THF = tetrahydrofuran). Particularly noteworthy is that this Table S1 shows that geometric differences of corresponding mean molecular metal−metal distances of **1** in **1a** and **1b** due to different solid-state solvation effects are small (≤0.05 Å) for the 27 different types of mean metal−metal distances. Table S1 also shows that the corresponding different atom-pair connectivities involving both the mean $\{Pd_4C\}$−Pd_{shell} and Pd_{shell}−Pd_{shell} distances in **1a** versus the mean Au_4−Pd_{shell} and Pd_{shell}−Pd_{shell} distances in **2a** are likewise small (≤0.07 Å).

(b) Structural Features of 1 and Comparative Analysis with 2. This nanosized cluster (**1**) possesses a tetracoordinated carbide atom that causes the interior tetrapalladium cage to be highly deformed from a regular tetrahedron into a new type of completely encapsulated $\{Pd_4C\}$ entity of pseudo-D_2 (222) symmetry. Mean distances for the three pairs of opposite twofold-equivalent Pd−Pd edges are 2.71, 2.96, and 3.59 Å for solvated crystal **1**·2.5 C_6H_{14} (**1a**) and 2.71, 2.99, and 3.60 Å for solvated crystal **1**·3 $CHCl_3$ (**1b**); the mean of the four Pd−C distances [range: 1.87(2)−1.94(2) Å in **1a**; 1.88(2)−1.94(2) Å in **1b**] in both **1a** and **1b** is 1.91 Å (Table 1), and the three mean Pd−C−Pd pair angles are 90.2°, 102.9°, and 140.6° (whereas the ideal tetrahedral angle is 109.5°). The view of **1** in Figure 1a shows that the three mutually perpendicular pseudo-C_2 axes, each passing through the central carbide atom and midpoints of two opposite Pd−Pd edges, are approximately oriented as horizontal and vertical in-plane C_2 axes and a perpendicular out-of-plane C_2 axis. This idealized D_2 $\{Pd_4C\}$-$Pd_{32}P_{14}$ geometry of **1** is preserved upon addition of the 28 bridging COs. Figure 2 provides comparative views (same as in Figure 1) of the entire molecular configurations of **1** and **2** (without methyl substituents), which clearly display their isostructural relationship that arises from analogous geometrical encapsulations by identical $Pd_{32}(CO)_{28}(PMe_3)_{14}$ shells of the electronically equivalent and structurally similar interior carbon-filled $Pd(i)_4$ cage and empty Au_4 cage, respectively. Both molecules in Figure 2 are shown in virtually identical

DOI: 10.1021/acs.inorgchem.5b00208
Inorg. Chem. XXXX, XXX, XXX−XXX

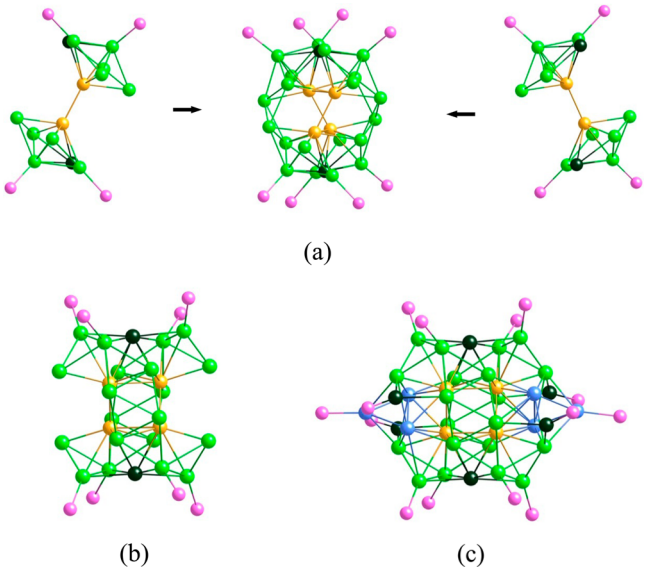

Figure 4. Previously proposed anatomy[7a] of nanosized $Au_4Pd_{32}P_{14}$ fragment (without COs) of $Au_4Pd_{32}(CO)_{28}(PMe_3)_{14}$ (**2**) envisioned to arise from the following: (a) Formation of twinned composite $Au_4Pd_{22}P_8$ kernel of **2** from interpenetration of two identical Au−Au bonded $Au_2Pd_{12}P_4$ dimers with vertex-fusion of two Pd (dark green). Resulting geometry consists of tetrahedrally deformed empty Au_4 cavity of pseudo-D_2 (222) symmetry with three pairs of opposite twofold-equivalent Au−Au edges: (1) intradimer electron-pair Au−Au bonding, 2.64 Å; (2) weak interdimer Au−Au bonding, 2.90 Å; (3) interdimer Au−Au nonbonding, 3.51 Å. This central $Au_4Pd_{22}P_8$ kernel is oriented with in-plane horizontal C_2 axis and in-plane vertical C_2 axis; the third perpendicular out-of-plane C_2 axis bisects midpoints of two intradimer electron-pair Au−Au bonds. (b) Another view of $Au_4Pd_{22}P_8$ kernel after 90° rotation about the in-plane vertically oriented C_2 axis. (c) Entire $Au_4Pd_{32}P_{14}$ architecture formed by addition of six blue-colored Pd and four exopolyhedral dark green Pd atoms with attached P atoms.

orientations to highlight (in particular) the extraordinary structural similarities in CO ligation. Their remarkable isostructural architectures point to similar formal geometrical sequences in growth patterns for **1** and **2** that are outlined in Figures 3 and 4, respectively.

The mean distances of the twofold-equivalent opposite pairs of its Pd−Pd edges of the $\{Pd_4C\}$ core in **1** are only 0.06−0.09 Å larger than those of the corresponding Au−Au edges of the Au_4 core in **2**. In addition to this nearly perfect size/shape geometrical match, the filled $\{Pd_4(\mu_4\text{-}C)\}$cage in **1** is electronically equivalent to the empty Au_4 cage in **2**. Consequently, geometrical encapsulations of the $\{Pd_4C\}$ entity in **1a**,**b** and of the Au_4 entity in **2** by identical $Pd_{32}(CO)_{28}(PMe_3)_{14}$ shells are analogous, in accordance with the Pd−Pd separations between Pd atoms of the $Pd(i)_4$ cage and atoms of the Pd_{32} shell differing by less than 0.1 Å from the corresponding Au−Pd separations in the Au_4Pd_{32} **2**. Therefore, aside from electronic factors (vide infra), it is then not completely surprising that the remarkably similar geometrical deformations found in both the electronically equivalent interior C-filled $Pd(i)_4$ and empty Au_4 cages are stabilized by the same $Pd_{32}(CO)_{28}(PMe_3)_{14}$ shells.

(c) Ligand Arrangements. The stereochemical dispositions (shown in Figure 2) of the PR_3/CO ligands in **1** virtually duplicate those found in **2**. All 14 Pd−P connectivities in **1** possess the same mean distance of 2.31 Å, as was found in **2** (Table S1). Of the 28 carbonyls in **1**, 20 are doubly bridging, and 8 are triply bridging; the mean Pd-(μ_2-CO) and Pd-(μ_3-CO) distances of 2.04 and 2.11 Å, respectively, in **1** are identical with those observed in **2** (Table S1).

Computational Analysis of $\{Pd_4(\mu_4\text{-}C)\}Pd_{32}(CO)_{28}(PH_3)_{14}$ (1-mod) and $Au_4Pd_{32}(CO)_{28}(PH_3)_{14}$ (2-mod). *(a) Methodology.* To gain an insight into the possible physical reasons behind the isostructural Pd and Pd−Au interiors in **1** and **2**, respectively, we performed a natural population analysis (NPA) of atomic charges in models of these molecules. The experimental geometries of the two fully ligated clusters **1** and **2** were used for the analysis with each trimethylphosphine ligand of the experimental structure being replaced by a PH_3 ligand for computational efficiency, namely, $\{Pd_4C\}Pd_{32}(CO)_{28}(PH_3)_{14}$ (**1-mod**) and $Au_4Pd_{32}(CO)_{28}(PH_3)_{14}$ (**2-mod**). The wavefunctions for further analysis were obtained by use of meta-GGA DFT functional M06L,[16] as implemented in Gaussian 09 A.01.[17] Gold and palladium atoms were described with the effective core potential (ECP) LANL2 combined with a modified double-ζ 18-valence-electron basis set DZ[18] on Au and Pd, while lighter atoms were treated with the Pople 6-31G* all-electron basis set.[19] Modifications in the Au and Pd valence basis sets involved reoptimized exponents for 6p and 5p orbitals, respectively, to account for more involved participation of these orbitals in bonding than previously assumed. All necessary geometry optimizations (see text) were performed by use of the SVWN5 local spin-density DFT functional[20] with the same basis set as described above. The modified NPA (including Wiberg bond-order evaluation) was conducted by the NBO5.9 procedure in Gaussian 09.

(b) Resulting Computational Implications. The NPA of the Pd_4C entity in **1-mod** expectedly reveals significant negative charge on the carbon atom and four electron-deficient bonds (1.67 electrons per bond) between the central carbon atom and each of the four palladium atoms formed by the $sp^{0.5}$ hybrid of the carbon atom and 5s orbital of each metal. The electron configuration of each palladium atom points to the noticeable 4d-to-5s promotion of ∼0.5 electrons per atom that is responsible for the described Pd−C bonding. The Wiberg bond-order index[21] also points to somewhat increased bond order between the closest palladium atoms: ∼0.35 "intradimer" bond order (BO) versus ∼0.12 "interdimer" BO (Table 2). Despite these differences in BO, the NPA suggests no major bonding interactions between the closely positioned palladium atoms.

An individual neutral Au_4 cluster has been previously predicted[22] to possess the geometry of an elongated rhombus with its short diagonal being smaller than its sides; the arrangement of four gold atoms observed in **2-mod** is estimated to be 20−25 kcal/mol higher in energy. Furthermore, such an arrangement is only slightly more stable (by 2 kcal/mol) than two noninteracting Au_2 dimers. From these energy arguments, it is likely that the electronic structure of the Au_4 core in **2** might resemble the superposition of two weakly interacting Au_2 dimers.

NPA reveals that the electronic structure of the individual Au_4 fragment can be envisioned as comprised of two weakly interacting Au_2 dimers in close proximity to each other. Two natural bonds were identified in the individual Au_4 core, with bonds between gold atoms in each dimer being the same as in the individual Au_2 dimer and formed primarily via interaction of unhybridized 6s NAOs of each gold atom, as the 5d NAOs of

DOI: 10.1021/acs.inorgchem.5b00208
Inorg. Chem. XXXX, XXX, XXX−XXX

Table 2. Electronic Configurations of Interior Metal (M) Core Atoms and Wiberg Bond Orders in (1-mod)-Bound Pd_4C Core and in (2-mod)-Bound Au_4 Core and in Corresponding Au_4 Core from 2-mod

core[a]	electronic configuration	intra-BO[b]	inter-BO[b]
Pd_4C in **1-mod**	$5s^{0.54}4d^{9.33}$tail(0.02)[c]	0.35	0.12
Au_4 from **2-mod**[d]	$6s^{1.06}5d^{9.96}6p^{0.02}$tail(0.00)	0.93	0.08
Au_4 core in **2-mod**	$6s^{1.18}5d^{9.84}6p^{0.01}$tail(0.09)[c]	0.17	0.03

[a]**1-mod** and **2-mod** designate isostructural model $\{Pd_4C\}Pd_{32}(CO)_{28}(PH_3)_{14}$ and $Au_4Pd_{32}(CO)_{28}(PH_3)_{14}$ clusters, respectively, of pseudo-D_2 symmetry (with P-attached Me substituents replaced by H atoms). Each interior M_4 entity may be envisioned as two identical M_2 intradimers (M = Pd, 2.71 Å in **1-mod**; M = Au, 2.64 Å in **2-mod**) that form under pseudo-D_2 symmetry two identical shorter diagonal interdimer bonding distances (M = Pd, 2.96 Å in **1-mod**; M = Au, 2.90 Å in **2-mod**) and two identical longer interdimer nonbonding distances (M = Pd, 3.59 Å in **1-mod**; M = Au, 3.51 Å in **2-mod**). [b]Intra-BO denotes Wiberg bond order of two identical intradimer M-M bonding distances; inter-BO denotes Wiberg bond order of two identical shorter M-M diagonal interdimer bonding distances. [c]Tail (0.02 or 0.09) in the electronic configuration implies the total occupation number in higher-energy AOs than 5s in Pd or 6p in Au. [d]Au_4 core per se.

each gold atom are almost fully occupied. The Wiberg bond order of 0.93 (for Au_4 from **2-mod**) clearly points to the existence of a single bond between two gold atoms in each dimer (Table 2), whereas its value of 0.08 for the bonding interdimer Au−Au interactions is relatively small. Table 3 shows that insertion of the Au_4 core into the $Pd_{32}(CO)_{28}(PH_3)_{14}$ shell (i.e., Au_4 in **2-mod**) gives rise to the transfer of almost 0.39*e* from the ligands (60% from PH_3 and 36% from CO) onto the gold core, thereby causing the core to acquire negative charge, similar to the Au_2 entity in the earlier reported Au_2Pd_{28} cluster $Au_2Pd_{28}(CO)_{26}(PR_3)_{10}$.[23] An analysis in Table 2 of the gold electron configuration in **2-mod** shows that more than half of the newly acquired electron density is located on Au(6s) NAO, whereas the remaining density occupies higher 6p, 7s AOs—the "tail" of the electronic configuration—further away from the atomic center. At the same time, the Au_4 incorporation in the **2-mod** interior further facilitates depletion of the 5d orbital whose occupation diminishes by 0.12*e*. A large decrease in the intradimer BO was also observed, from 0.93 to 0.17, caused by considerable electron-density Au−Pd_{shell} delocalization within the cluster core due to extensive Pd_{shell} coordination. Nevertheless, the significant difference between intradimeric and interdimeric Wiberg bond orders points to the bonding anisotropy being retained within the Au_4 entity.

An analysis of electron-density deformation $\Delta\rho$ leads to the same conclusion about two weakly interacting gold dimers in **2-mod** (Figure S1). The deformation of electron density was calculated by subtraction of the individual Au_4 core electron density and the electron density of the model "shell" cluster $Pd_{32}(CO)_{28}(PH_3)_{14}$ from the electron density of the complete cluster **2-mod**: $\Delta\rho = \rho(\textbf{2-mod}) - \rho(Au_4) - \rho(Pd_{32}(CO)_{28}(PH_3)_{14})$. As the interaction between Au_4 and the cluster shell "turns on", the buildup of the electron density in the intradimer space outside the core in line with the Au−Au intradimer bond is apparent [Figure S1a,b], which is consistent with the accumulation of the negative charge on the Au_4 core established from the NPA (Table 3). The extension of significant deformation density outside of the core along the Au−Au connectivity vector is consistent with an increased population of higher NAOs on gold, which is also apparent from significant combined population of 6p and higher orbitals, totaling 0.09 electrons per atom (Table 2). The maximum $\Delta\rho$ in the intradimer region is 664×10^{-5} e/Å^3. No bond-density buildup is apparent in the interdimer space, with maximum $\Delta\rho$ found to be only 12×10^{-5} e/Å^3. Similar anisotropy in deformation of electron density is observed if the Au_4 core is simply placed between four intradimer oriented PH_3 ligands, essentially creating two weakly interacting $Au_2(PH_3)_2$ dimers (Figure S1b): the presence of donor ligands increases the electron density in the intradimer space up to 760×10^{-5} e/Å^3, whereas the maximum increase of electron density between dimers is 216×10^{-5} e/Å^3, which occurs at the centroid of the Au_4 fragment. Such anisotropic deformation of electron density clearly points to the existence of two weakly bound Au_2 dimers in **2-mod** rather than a single Au_4 core with delocalized bonding.

Table 3 discloses that ∼50% of the negative-charge buildup on Pd_4C in **1-mod** originates from the cluster Pd_{32} surface metal shell, in contrast to only 3% of the charge increase on Au_4 in **2-mod** from an identical Pd_{32} shell. This shift in the source of the cluster core negative-charge buildup from primarily the Pd_{32} metal shell (in **1-mod**) toward the ligands (in **2-mod**) may

Table 3. Natural Atomic Charges on Metallic Fragments and Ligands (Atomic, *q*, and Entire Molecular Group, *Q*) in Complete Clusters 1-mod and 2-mod and in These Clusters with the Interior Pd_4C and Au_4 Entity, Respectively, Removed (Same Cluster Shell)[a]

charge	**1-mod** shell	**1-mod** complete	Δ%[b]	**2-mod** shell	**2-mod** complete	Δ%[b]	$Au_4(PH_3)_4$
Q(cluster interior)		−0.609			−0.386		−0.194
$q(M_{int})$[c]		−0.033			−0.097		−0.049
$q(C_{int})$		−0.479					
$Q(Pd_{32}$ surface)	+3.262	+3.571	50.7	+3.191	+3.204	3.3	
$q(Pd_{surface})$[c]	+0.102	+0.111		+0.100	+0.100		
Q(CO)	−5.347	−5.167	29.6	−5.249	−5.109	36.3	
q(CO)[c]	−0.191	−0.185		−0.187	−0.182		
$Q(PH_3)$	+2.085	+2.205	19.7	+2.058	+2.291	60.3	+0.194
$q(PH_3)$[c]	+0.149	+0.158		+0.147	+0.164		

[a]**1-mod** and **2-mod** designate model $\{Pd_4C\}Pd_{32}(CO)_{28}(PH_3)_{14}$ and $Au_4Pd_{32}(CO)_{28}(PH_3)_{14}$ clusters, respectively, with electronically equivalent $\{Pd_4C\}$ or Au_4 embedded within an identical surface $Pd_{32}(CO)_{28}(PH_3)_{14}$ shell model. [b]Δ% is the percentage of charge adjustment on each molecular group upon removal of these interior fragments from the corresponding complete cluster. For comparison, charges on analogously deformed $Au_4(PH_3)_4$ are shown in the last column. [c]$q(M_{int})$, $q(Pd_{surface})$, *q*(CO), $q(PH_3)$ denote metal (M) or ligand per unit.

DOI: 10.1021/acs.inorgchem.5b00208
Inorg. Chem. XXXX, XXX, XXX−XXX

explain how the introduction of gold atoms into a palladium catalyst modifies the selectivity of the homopalladium catalyst. Most likely, such shifts arise from the lower energies of gold valence orbitals compared to those of palladium orbitals and their more efficient coupling with those of phosphine ligands, thereby yielding *more efficient* charge transfer from the ligands onto the metal cluster Au−Pd core.

Topological analyses of electron density within the Pd_4C and Au_4 cores in **1-mod** and **2-mod** present another approach to identify bonding interactions in the two cores. This analysis of $Pd_4(\mu_4\text{-}C)$ core (shown in Figure 5a) revealed only four calculated (3, −1) bond critical points (BCPs) corresponding to Pd−C bonding but no BCPs between Pd atoms. [Noteworthy is that a (3, −1) BCP is a point located between two atoms in which the electron density is a minimum in the direction of the bonded atoms and a maximum in the two orthogonal directions; it is taken as indicative of covalent bonding.] The analysis of electron density in Pd_4C core identifies very small but negative values of energy density at the midpoints between adjacent Pd atoms that suggest uniformly weak interpalladium interactions. In contrast, QTAIM analysis of the individual Au_4 core in **2-mod** identified four (3, −1) BCPs (Figure 5b) that are located midway between two gold atoms of the two Au_2 intradimers and midway between the two Au_2 bonding interdimers, namely, two BCPs 1 and two BCPs 2, respectively. In addition, one (3, +1) ring critical point (RCP) was identified close to the fragment's centroid (Figure 5b). The two sets of BCPs in the Au_4 core in **2-mod** indicate that interdimeric Au_2 bonding is also significant. The different locations of the BCPs in the $Pd_4(\mu_4\text{-}C)$ core versus those in the Au_4 core provide additional definite evidence concerning their dissimilar bonding scenarios in spite of their remarkable geometrical/electronic equivalences.

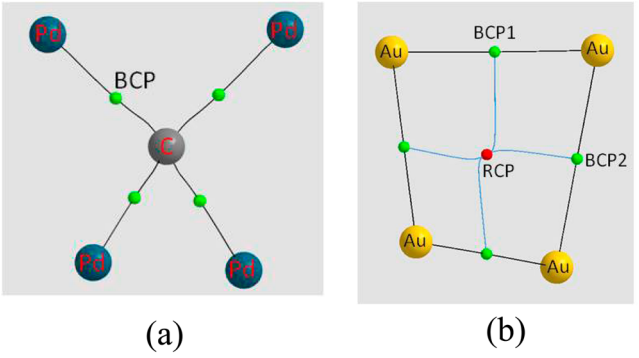

Figure 5. (a) Calculated model of Pd_4C cluster core in **1-mod** with ρ BCP critical points (green) together with bonding paths. (b) Calculated model of Au_4 cluster core in **2-mod** with ρ critical points—BCP1 and BCP2 (green) and the RCP (red)—together with bonding paths and RCP-to-BCP paths.

Comparative Analysis of Mean Pd−C Distance in 1 with Those in Known Palladium-Containing Mixed-Metal Carbide Clusters. Because **1** is the first example of a cluster with a tetracoordinated carbide atom exclusively encapsulated within a homopalladium cage, of interest is a comparison of its mean Pd−C bonding connectivities with those in heteropalladium carbide clusters having at least one Pd−C bond. To our knowledge, all such previously characterized bimetallic/trimetallic heteropalladium carbide clusters are known only for Fe, Co (or Fe/Co), Ru, and Os

Table 4. $Pd-C_{carbide}$ Mean Distances (Å) in Palladium-Containing Mixed-Metal Carbide Clusters with the Mono-Interstitial C Atom(s) Either in the Distorted Trigonal Bipyramidal $PdM_4(\mu_5\text{-}C)$ or in the Distorted Octahedral $Pd_xM_{6-x}(\mu_6\text{-}C)$ Cages, where M and x are Specified in the Table

entry	cluster	environment of carbido atom	mean Pd−C distance	reference
1	$\{Os_4C(CO)_{10}(\mu\text{-}Cl)(\mu\text{-}PPh_2py)\}(\mu_4\text{-}Pd)\ \{Os_4C(CO)_{12}(\mu\text{-}Cl)\}$[a]	$[PdOs_4(\mu_5\text{-}C)]$	2.04	24a
2	$\{Os_4C(CO)_{12}(\mu\text{-}Cl)\}_2(\mu\text{-}Pd_2Cl_2)$	$[PdOs_4(\mu_5\text{-}C)]$	1.99	24a
3	$\{Os_4C(CO)_{12}(\mu\text{-}I)\}_2(\mu\text{-}Pd_2I_2)$	$[PdOs_4(\mu_5\text{-}C)]$	1.99	24a
4	$PdOs_5C(CO)_{15}(\mu\text{-}Cl)_2(PPh_3)$	$[PdOs_4(\mu_5\text{-}C)]$	2.04	24b
5	$PdFe_3CoC(CO)_{12}(\eta^3\text{-}C_3H_5)$	$[PdFe_3Co(\mu_5\text{-}C)]$	2.01	24c
6	$HPdFe_2Ru_2C(CO)_{12}(\eta^3\text{-}C_{10}H_{15})$[b]	$[PdFe_2Ru_2(\mu_5\text{-}C)]$	2.00[c]	24d
7	$Pd_8Ru_{10}C_2(CO)_{27}(C_3H_5)_4$	$[PdRu_5(\mu_6\text{-}C)]$	2.03	24e; CCDC Refcode LISVEO[25]
8	$PdRu_5C(CO)_{15}(P^tBu_3)$	$[PdRu_5(\mu_6\text{-}C)]$	2.10	24f
9	$Pd_2Ru_5C(CO)_{15}(P^tBu_3)_2$	$[PdRu_5(\mu_6\text{-}C)]$	2.13	24f
10	$PdOs_5C(CO)_{14}(\mu\text{-dppf})$[d]	$[PdOs_5(\mu_6\text{-}C)]$	2.04	24g
11	$Pd_4Os_5C(CO)_{15}(\mu\text{-dppm})_2$[e]	$[PdOs_5(\mu_6\text{-}C)]$	2.00	24h; CCDC Refcode PUNVEZ[25]
12	$Pd_2Fe_3RuC(CO)_{12}(\eta^3\text{-}C_{10}H_{15})_2$[b]	$[Pd_2Fe_3Ru(\mu_6\text{-}C)]$	2.12	24i
13	$[H_{3-n}Co_{15}Pd_9C_3(CO)_{38}]^{n-}$	$[PdCo_5(\mu_6\text{-}C)]$		24j
	n = 0		1.99	
	n = 1		1.99	
	n = 2		2.03	
	n = 3		2.00	
	$[H_{6-n}Co_{20}Pd_{16}C_4(CO)_{48}]^{n-}$	$[PdCo_5(\mu_6\text{-}C)]$		24k
	n = 4		2.03	
	n = 5		1.96	
14	$Co_4Pd_2C(CO)_{11}(PPh_3)_2$	$[Pd_2Co_4(\mu_6\text{-}C)]$	2.14	24k
15	$Co_2Pd_5C(CO)_8(PPh_3)_5$	$[Pd_4Co_2(\mu_6\text{-}C)]$	2.10	24k

[a]PPh_2py = diphenyl-2-pyridylphosphine. [b]$\eta^3\text{-}C_{10}H_{15}$ = η^3-β-pinenyl. [c]For two crystallographically independent molecules. [d]dppf = 1,1′-bis(diphenylphosphino)ferrocene. [e]dppm = bis(diphenylphosphino)methane.

DOI: 10.1021/acs.inorgchem.5b00208
Inorg. Chem. XXXX, XXX, XXX−XXX

and involve carbide-encapsulated metal cages with either five or six metal atoms. These clusters along with the compositions of their metal cages and mean Pd−C distances are presented in Table 4. As expected, their syntheses are more complex than that for **1**.

The mean value of 1.91 Å for the Pd-(μ_4-C) distance in the two structures of **1** determined in **1a** and **1b** (Table 1) is 0.10 Å smaller than the mean Pd-(μ_5-C) distance of 2.01 Å (mean range, 1.99−2.04 Å) for the six listed pentacoordinated heteropalladium carbide clusters (in Table 4) and likewise is 0.14 Å smaller than the mean Pd-(μ_6-C) distance of 2.05 Å (mean range, 1.96−2.14 Å) for the 14 listed hexacoordinated heteropalladium carbide clusters (in Table 4). This bond-length trend is completely consistent with an enlargement of the metal cage size upon incorporation of a greater number of metal cage atoms coupled with the size restrictions (i.e., a constraint matrix effect) imposed upon the Pd(μ_4-C) cage by the encapsulating Pd_{32} shell (vide supra).

Comparison of 1 with Known $M_4(\mu_4$-C) Clusters Containing a Carbido Atom Tetracoordinated to Four Metals. Highly distorted tetrahedral arrangements of four metal atoms around a carbide atom by itself is not at all surprising. But a carbide atom cannot be geometrically accommodated inside of a regular (nondistorted) tetrahedral metal cage with retention of all six metal−metal bonds.[2] Known examples of a C atom coordinated to four metal centers include more-or-less deformed metal tetrahedra either with all six M−M bonds broken, [e.g., $M_4(\mu_4$-C) with M = Hg,[26a,b] Pb,[26c] Sn,[26d] Ge,[26e] Au;[26f] M_4 = Al_3Ti,[26g,h] Al_2Ti_2[26i]] or with deformed metal tetrahedra possessing one to three significantly weakened or broken M−M bonds. Among this second group are the long-known "butterfly"-based clusters containing a linear M−C−M arrangement (i.e., with one broken M−M bond)[2] with an exposed C atom, and a few $M_4(\mu_4$-C) clusters with two or three highly elongated or broken M−M bonds. Examples are a pentametal-bonded butterfly $WOs_3(\mu_4$-C) cluster of formula $WOs_3(\mu_4$-C)$(\mu_2$-H)$_2(\eta^5$-$C_5H_5)$(CO)$_9(\mu_2$-SMe)[27] with a linear W−C−Os architecture, another tetrametal-bonded $WOs_3(\mu_4$-C) cluster of formula $WOs_3(\mu_4$-C)$(\eta^5$-$C_5H_5)$(CO)$_{11}(\mu_2$-SMe)[27] with nonbonding W···Os and Os···Os distances, and a trimetal-bonded $RuCo_3(\mu_4$-C) cluster[28] with a tetrahedral sp^3 carbide atom. This latter $RuCo_3(\mu_4$-C)$(\eta^5$-$C_5H_5)$(CO)$_8L_3$ cluster[28] is the first crystallographic example of a tetrahedral sp^3 carbide cluster with the (μ_4-C) atom coordinated to a trimetal-bonded $Co_3(CO)_6L_3$ fragment [where L_3 denotes tdpm $CH(PPh_2)_3$] and to an otherwise nonbonded Ru(η^5-C_5H_5)$(CO)_2$ moiety. An unusual example of a tetrametal-bonded butterfly-based $M_4(\mu_4$-C) cluster with two broken M−M bonds is the $Ru_2Pt_2(\mu_4$-C) cluster of formula $Ru_2Pt_2(\mu_4$-C)$(\mu_2$-H)$_2(\eta^5$-$C_5H_5)_2$-$(CO)_2(P^iPr_3)_2$[29] that is folded about the linear Ru−C−Ru axis; however, the resulting highly elongated Pt−Pt separation of 3.132(1) Å implies little or no direct metal−metal bonding. Particularly noteworthy is that closed-shell electronic metal configurations are achieved in these $M_4(\mu_4$-C) metal carbide clusters.

An exceptional geometrical arrangement was observed for the $W_4(\mu_4$-C) framework in the $[W_5(C)I_{13}]^-$ anion ($[NBu_4]^+$ counterion);[30] unlike all other known metal-bonded square-pyramidal $M_5(\mu_5$-C) clusters for which the pentacoordinated (μ_5-C) atoms approximately reside within the basal tetrametal frameworks, the tetracoordinated (μ_4-C) carbide atom is 1.06 Å below the square-basal W_4 plane at 2.98 Å from the axial octahedrally coordinated W atom compared to its normal basal W−C bonding distances of 2.09(4)−2.24(3) Å.

From symmetry considerations, the only tetrametal-coordinated carbide cluster that is structurally related to **1** is the $[Re_4(\mu_4$-C)$(CO)_{15}I]^-$ anion (as the $[PPN]^+$ salt),[31] which was reported in 1985 in very low yield from a partial oxidative fragmentation of the monocapped octahedral carbido $[Re_7(\mu_6$-C)$(CO)_{21}]^{3-}$ anion by reaction with I_2 in MeCN under CO atmosphere. An X-ray crystallographic determination of this $[Re_4(\mu_4$-C)$(CO)_{15}I]^-$ anion showed four octahedrally coordinated Re atoms [namely, one $Re(CO)_3I$ and three $Re(CO)_4$ fragments] that are each linked to one another in a cyclic cis-fashion via two Re−Re single bonds. The additional attachment of these four Re atoms to the carbido atom gives rise to a central $Re_4(\mu_4$-C) entity of pseudo-D_{2d} ($\bar{4}2m$) symmetry with two mean Re−C−Re trans bond angles of 157.4° and four mean Re−C−Re cis bond angles of 92.1°, indicating that the carbido atom is much closer to square-planar instead of tetrahedral Re−C coordination; although exposed, the carbide atom is sterically protected by the axial octahedral Re ligands. The central $Re_4(\mu_4$-C) entity of pseudo-D_{2d} symmetry thereby geometrically differs from the pseudo-D_2 isostructural $Pd_4(\mu_4$-C) and Au_4 entities in **1** and **2**, respectively, in possessing two instead of three kinds of symmetry-equivalent M−M connectivities, namely, four equivalent opposite single-bond Re−Re (rhombus) edges (mean, 3.00 Å) and two equivalent nonbonding diagonal Re···Re distances (mean, 4.09 Å). Both its structure and composition conform to a closed-shell electronic metal configuration.

Geometric Comparison with Only Other Known Nanosized Au−Pd Cluster $Au_4Pd_{28}(CO)_{22}(PMe_3)_{16}$ Possessing a Tetragold Kernel. A previous study[32] showed that analogous precursors under different reaction conditions produced another new type of tetragold−palladium cluster, $Au_4Pd_{28}(CO)_{22}(PMe_3)_{16}$ (**6**), that not only has a completely dissimilar Au_4Pd_{28} core geometry with a nearly regular encapsulated Au_4 tetrahedron but also a totally different postulated multitwinned composite growth pattern. This cluster, which was obtained from the reaction of $Pd_{10}(CO)_{12}$-$(PMe_3)_6$ with Au(SMe_2)Cl or Au(PPh_3)Cl (yield, ∼20−40%), has a 32 metal-atom Au_4Pd_{28} framework that conforms to pseudo-cubic T (23) symmetry, which is reduced to general C_1(1) symmetry upon inclusion of its 22 bridging CO ligands.

A comparative analysis of resulting low-temperature CCD X-ray diffractometry determinations[32] of two different solvated crystals of **6** revealed an amazing molecular similarity that clearly indicates that the observed analogous geometrical distortions are primarily induced by intracluster strain-releasing effects and not by crystal-packing interactions. A multitwinned growth-pattern of its Au_4Pd_{28} core was proposed involving the formation of a Au_4Pd_{24} composite-twinned architecture formed from four markedly deformed interpenetrating three-layer Au(n)-centered $[Pd_3]_A[Au(n)Pd_6]_B[Au_3]_C$ cuboctahedra (n = 1−4) that are oriented along the four localized threefold axes of the encapsulated Au_4 tetrahedron; the remaining four outermost (external) Pd atoms are tetrahedrally disposed about the Au_4Pd_{24} composite and presumably provide stabilization via face condensations (specifically, three tetracapped; one tricapped). The mean Au−Au distances of the Au_4 tetrahedron in **6**·^{i}Pr_2O and **6**·5THF·hexane are 2.75 and 2.77 Å (ranges, 2.648(1)−2.810(1) Å; 2.687−2.823(1) Å).[32]

Relevance to Heterogeneous Pd and Pd/Au Catalysts for Conversion of Ethylene to Vinyl Acetate. Palladium

DOI: 10.1021/acs.inorgchem.5b00208
Inorg. Chem. XXXX, XXX, XXX−XXX

has long been widely used as a heterogeneous catalyst for the multiton production of such an important monomer as VA, which is formed by oxidation of ethylene in the presence of acetic acid.[6a] The fact that Pd−Au catalysts were shown to exhibit much higher reactivities than Pd-based catalysts in VA synthesis led to a comprehensive investigation[6b−f] as to whether Pd−Au catalysts resist carbide formation; it was concluded that there is no evidence for PdC_x entities in a Pd−Au alloy following VA synthesis such that the alloying of Au with Pd is apparently very effective in preventing PdC_x formation in Pd-based catalysts for VA synthesis.

CONCLUSIONS

The first homopalladium carbido cluster, $\{Pd_4(\mu_4\text{-}C)\}Pd_{32}(CO)_{28}(PMe_3)_{14}$ (**1**), was obtained via an ultimately simplified straightforward reaction of either $Pd_8(CO)_8(PMe_3)_7$ or $Pd_{10}(CO)_{12}(PMe_3)_6$ with $CHCl_3$ at room temperature under N_2. X-ray crystallographic determinations of solvated crystals (**1a** and **1b**) of **1** at 100 K revealed closely related structures consisting of a highly unusual tetracoordinated C atom encapsulated within a highly distorted tetrahedral Pd_4 cage of pseudo-D_2 symmetry. The unprecedented $\{Pd_4C\}$ kernel in **1a** may be described as two symmetry-equivalent Pd_2 intradimers (mean, 2.71 Å) that are linked to each other by a weakly bonding interdimer Pd_2 pair (mean, 2.96 Å); the other interdimer Pd_2 pair is nonbonding (mean, 3.59 Å). The mean of the four Pd−C distances is 1.91 Å [range, 1.87(2)−1.94(2) Å], and mean values for the three pairs of opposite tetrahedrally deformed Pd−C−Pd bond angles are 90.2°, 102.9°, and 140.6°.

A completely unanticipated and prime feature is that the molecular geometry of **1** is essentially isomorphic with that in the known $Au_4Pd_{32}(CO)_{28}(PMe_3)_{14}$ (**2**), in which an identical Pd_{32} shell analogously accommodates a Au_4 kernel that is geometrically similar in size and shape and is electronically equivalent to the $\{Pd_4C\}$ kernel in **1**. Mean distances for the three corresponding symmetry-equivalent pairs of opposite tetrahedrally deformed Au−Au edges within the Au_4 kernel in **2** are 2.64, 2.91, and 3.51 Å. However, the NPA and AIM method indicated that the bonding interactions of **1-mod** and **2-mod**, respectively (in which P-attached Me substituents were replaced by H atoms), are different. Whereas the two Pd_2 dimers in the negatively charged $\{Pd_4C\}$ entity in **1** are primarily stabilized by Pd−C interactions, the corresponding Au_2 dimers in **2** are stabilized by direct Au−Au bonds. The NPA also showed that both the Pd_{32} shell and its ligands play a crucial role in the tuning of overall similar negative electron densities upon $\{Pd_4C\}$-for-Au_4 substitution. This interchangeable accommodation of the negatively charged $\{Pd_4C\}$ and Au_4 entities offers a reasonable explanation of why the Au-doped Pd catalyst used for the oxidation of ethylene into vinyl acetate (in the presence of acetic acid) prevents carbidization, namely, the valence 6s Au electron of each added gold atom provides an efficient "negative charge protection" against the formation of negatively charged palladium carbide species such as $\{Pd_4C\}$ obtained from electron-donating carbon atoms.

EXPERIMENTAL SECTION

Synthesis and IR Spectroscopic Characterization of $\{Pd_4C\}Pd_{32}(CO)_{28}(PMe_3)_{14}$ (1). *General Remarks.* The standard Schlenk technique was used for performing all reactions. Solvents were deoxygenated by the passage of N_2 through them for at least 20 min prior to their use. The syntheses of $Pd_{10}(CO)_{12}(PMe_3)_6$ and $Pd_8(CO)_8(PMe_3)_7$ are analogous to that of $Pd_{10}(CO)_{12}(P^nBu_3)_6$ with an adjusted stoichiometry of Pd/P = 8/7 for the second one.[33] $Pd_{10}(CO)_{12}(PMe_3)_6$ was purified by recrystallization from C_6H_6/heptane. Infrared spectra were recorded on a Mattson Polaris FT-IR spectrometer; nujol mulls were prepared under nitrogen.

Pseudo-polymorphic crystals of **1** (i.e., different crystal types as the result of diverse solvation) were obtained from both $Pd_8(CO)_8(PMe_3)_7$ and $Pd_{10}(CO)_{12}(PMe_3)_6$ clusters via crystallizations of their $CHCl_3$ solutions in the presence of hexane vapor. The crystal shapes varied from blocks to thin plates and rods, whereas crystal solvations varied from hexane to $CHCl_3$ molecules; mixed hexane/$CHCl_3$ compositions of solvated molecules were found in **3a**. IR spectra of crystalline pseudo-polymorphs of **1** exhibited bridging carbonyl bands at 1880−1878 (s), 1868−1864 (sh), 1849−1806 (several sh bands), 1765−1743 (usually two distinguished m bands) cm^{-1}. For bulky samples bridging carbonyl bands at 1905−1900 (sh) and terminal 2031−2015 (mw-vw) cm^{-1} were also observed and attributed to contaminations. Dichloro-bis(trimetylphosphine)palladium(II) was identified by single-crystal X-ray diffraction as the cis-isomer in the form of two crystal types, namely, *cis*-$PdCl_2(PMe_3)_2 \cdot CHCl_3$ (**5a**) and nonsolvated *cis*-$PdCl_2(PMe_3)_2$ (**5b**).

*Synthesis of $1{\cdot}2.5C_6H_{14}$ (**1a**) from $Pd_8(CO)_8(PMe_3)_7$.* A solution of $Pd_8(CO)_8(PMe_3)_7$ (200 mg; 0.124 mmol) in 4 mL of $CHCl_3$ was kept under N_2 for 1 d, filtered, and left in the presence of hexane vapor. After two weeks 12 mg (7%) of black crystals of $\{Pd_4C\}Pd_{32}(CO)_{28}(PMe_3)_{14}{\cdot}2.5C_6H_{14}$ were decanted from amorphous Pd black. Its IR spectrum in nujol displayed the following carbonyl bands: 2015 (vw), 1878 (vs), 1864 (sh), 1845 (sh), 1828 (sh), 1816−1809 (sh, br), 1760 (m), 1743 (m) cm^{-1}. This IR spectrum is very close to the nujol spectrum of the isostructural and electronically equivalent Au−Pd cluster $Au_4Pd_{32}(CO)_{28}(PMe_3)_{14}$.[7a] A crystal of size 0.33 × 0.10 × 0.07 mm^3 was chosen for X-ray data collection.

Crystals of **1** with significantly less solvated hexane molecules [i.e., $1{\cdot}0.8C_6H_{14}$ (**1c**)] were obtained (estimated yield 1−2 mg) in an analogous synthesis but with crystallization set up immediately after the dissolving of the Pd_8 cluster. The unit cell triclinic crystal parameters for **1c** are a = 16.189(2) Å, b = 17.829(2) Å, c = 27.777(4) Å, α = 82.693(2)°, β = 75.197(2)°, γ = 83.783(2)°; V = 7664.3(18) $Å^3$. In addition to $1{\cdot}0.8C_6H_{14}$ (**1c**), colorless crystals of $PdCl_2(PMe_3)_2$ and dark red crystals of the precursor $Pd_8(CO)_8(PMe_3)_7$ [identified by an IR spectrum, nujol, carbonyl bands: 1875 (s), 1839 (m), 1819 (sh), 1808 (s), 1798 (sh), 1774 (m), 1761 (mw) cm^{-1}][11] were also obtained.

In striking contrast to the stability of crystals of $1{\cdot}2.5C_6H_{14}$ (**1a**), crystals of $1{\cdot}0.8C_6H_{14}$ (**1c**) at room temperature in absence of mother liquid were extremely fragile and readily self-destructed via explosion. X-ray data collection was accomplished only because the crystal was immediately transferred from the crystallization flask into the diffractometer nitrogen flow at 100 K; nevertheless, the $R_1(F)$ value of 0.12 was still high.

*Synthesis of $1{\cdot}3CHCl_3$ (**1b**) from $Pd_8(CO)_8(PMe_3)_7$ and $Pd_{10}(CO)_{12}(PMe_3)_6$.* This synthesis was analogous to the preparation of **1a**, but the solution was held under N_2 for 4 d, filtered from Pd black, and crystallization was then set up. It was completed in 9 d with the formation of 5 mg (3%) of black rodlike crystals of **1b** and 80 mg (18%) of light yellow large block crystals of *cis*-$PdCl_2(PMe_3)_2{\cdot}CHCl_3$ (**5a**). IR of **1b** in nujol, carbonyl bands: 1878 (s), 1868 (sh), 1847−1840 (sh), 1827−1806 (sh br), 1762 (w), 1743 (mw) cm^{-1}. The sizes of crystals selected for X-ray data collection were 0.26 × 0.08 × 0.05 mm^3 and 0.36 × 0.30 × 0.20 mm^3 (cut) for **1b** and **5a**, respectively. Crystals of **5a** exposed to air at room temperature quickly became cloudy due to loss of solvate molecules.

Crystals of **1b** were also obtained by a procedure analogous to that used for the preparation of **1a** but with $Pd_{10}(CO)_{12}(PMe_3)_6$ (190 mg; 0.102 mmol) as a precursor. Yields: **1b**, black crystals, ∼5 mg (3%); *cis*-$PdCl_2(PMe_3)_2$ (**5b**), colorless crystals, ∼15 mg (4%). IR of **1b**, (prepared from $Pd_{10}(CO)_{12}(PMe_3)_6$) in nujol, ν(CO): 1880 (s), 1866 (sh), 1849 (sh), 1833−1806 (sh br), 1765−1745 (mw br) cm^{-1}; unit cell triclinic crystal parameters: a = 16.0645(11) Å, b = 17.7303(13) Å,

DOI: 10.1021/acs.inorgchem.5b00208
Inorg. Chem. XXXX, XXX, XXX−XXX

c = 25.7442(18) Å, α = 87.681(1)°, β = 80.989(1)°, γ = 80.008(1)°; V = 7131.7(9) Å^3.

cis-$PdCl_2(PMe_3)_2$ (**5b**) was identified by comparison of its unit cell parameters, obtained by X-ray diffraction from a single crystal at 100 K (monoclinic, a = 6.264(2) Å, b = 11.793(4) Å, c = 8.747(4) Å; β = 110.69(2)°, V = 604.5(3) Å^3), with those from previous crystals measured at 273 K (specifically, monoclinic, a = 6.350(4) Å, b = 11.837(9) Å, c = 8.813(7) Å; β = 109.85(6)°, V = 623.0(8) Å^3).[34]

Crystals of **1** were sufficiently insoluble in common solvents such that no NMR spectra of **1** were obtained.

X-ray Crystallographic Determinations of $\{Pd_4C\}Pd_{32}(CO)_{28}(PMe_3)_{14}\cdot 2.5C_6H_{14}$ (1a), $Pd_{36}(\mu_4\text{-}C)(CO)_{28}(PMe_3)_{14}\cdot 3CHCl_3$ (1b) and *cis*-$PdCl_2(PMe_3)_2\cdot CHCl_3$ (5a). *General Remarks.* X-ray data were collected at 100(2) K with a Bruker SMART CCD-1000 area detector diffractometer and a Mo sealed-tube generator. Reflections in all data sets were empirically corrected for absorption (SADABS). The crystal structures were obtained by use of direct methods followed by successive Fourier difference maps. Least-squares refinements (based on F^2) were performed with SHELXL.[35]

In structures **1a**, **1b**, and **5a** all non-hydrogen atoms [other than those of solvated hexane molecules (**1a**), disordered solvated $CHCl_3$ molecule (**1b**), and disordered methyl carbon atoms of trimethylphosphine ligand (**1a** and **5a**)] were refined with anisotropic displacement parameters. In **1a**, methyl groups attached to P8, P12, and P14 atoms are disordered over two sites around each of the P atoms, with occupancy factors of 0.54/0.46, 0.72/0.28, and 0.71/0.29, respectively. One of the solvated hexane molecules in **1a** has $C_i(-1)$ site symmetry and thereby contributes half of molecule per cluster. The other two hexane molecules occupy general positions with one molecule disordered over two nearby sites with an occupancy factor of 0.61/0.39. In the crystal structure of **1b** all three solvated $CHCl_3$ molecules reside on general positions; one of these molecules is disordered over two sites with an occupancy factor of 0.74/0.26.

Distance restraints were applied for disordered Me groups and solvated molecules. Restraints on anisotropic displacement parameters of carbido atoms were imposed in both structures **1a** and **1b** to avoid nonpositive definite thermal parameters. EADP constraints and/or SIMU and DELU restraints were also used for solvated hexane molecules in **1a** and for a few light atoms in **1b**. Hydrogen atomic positions were generated geometrically and refined with a riding model. The largest residual peaks for all structures were located in close vicinities to peaks for Pd atoms and thereby were unambiguously assigned to systematic error (noise). For **5b** only unit cell parameters were determined (vide supra).

Structural tests performed by the checkCIF/PLATON service [via http://journals.iucr.org/services/cif/checking/checkform.html] are in agreement with the space groups chosen for these crystal structures and did not show any serious or unexpected problems. Additional crystallographic information, including details of structure refinements in cif files, is available in Supporting Information.

$Pd_{36}(\mu_4\text{-}C)(CO)_{28}(PMe_3)_{14}\cdot 2.5C_6H_{14}$ (1a). $C_{86}H_{161}O_{28}P_{14}Pd_{36}$: M = 5907.13 g·mol^{-1}; triclinic; $P\bar{1}$; Z = 2; a = 16.0206(11) Å, b = 17.7225(12) Å, c = 27.6060(19) Å, α = 82.698(1)°, β = 75.289(1)°, γ = 83.801(1)°; V = 7496.2(9) Å^3; d(calc) = 2.617 Mg/m^3; F(000) = 5534. Reflections (59591) obtained over 3.52 ≤ 2θ ≤ 52.00 (98.5% completeness at maximum 2θ); max/min transmission coefficients, 0.7484/0.3249; μ(Mo Kα) = 4.394 mm^{-1}. Full-matrix least-squares refinement on 29 018 independent merged (R(int) = 0.0572) reflections (1402 parameters, 126 restraints) converged at $wR_2(F^2)$ = 0.1506 for all data; $R_1(F)$ = 0.0589 for $I > 2\sigma(I)$; GOF (on F^2) = 0.912; max/min residual electron density, 1.840 and −1.351 e·A^{-3}.

$Pd_{36}(\mu_4\text{-}C)(CO)_{28}(PMe_3)_{14}\cdot 3CHCl_3$ (1b). $C_{74}H_{129}Cl_9O_{28}P_{14}Pd_{36}$: M = 6049.80 g·mol^{-1}; triclinic $P\bar{1}$; Z = 2; a = 16.0975(16) Å, b = 17.7114(17) Å, c = 25.768(3) Å, α = 87.771(2)°, β = 81.185(1)°, γ = 80.053(1)°; V = 7150.2(12) Å^3; d(calc) = 2.810 Mg/m^3; F(000) = 5632. Reflections (90 528) obtained over 3.38 ≤ 2θ ≤ 56.74 (95.4% completeness at maximum 2θ); max/min transmission coefficients, 0.7963/0.3700; μ(Mo Kα) = 4.773 mm^{-1}. Full-matrix least-squares refinement on 34 207 independent merged (R(int) = 0.0528) reflections (1438 parameters, 72 restraints) converged at $wR_2(F^2)$ = 0.2073 for all data; $R_1(F)$ = 0.0738 for $I > 2\sigma(I)$; GOF (on F^2) = 1.329; max/min residual electron density, 2.878 and −2.705 e·A^{-3}.

cis-$PdCl_2(PMe_3)_2\cdot CHCl_3$ (5a). $C_7H_{19}Cl_5P_2Pd$: M = 448.81 g·mol^{-1}; monoclinic; $P2_1/c$; Z = 8; a = 10.1667(7) Å, b = 28.1052(19) Å, c = 11.6394(8) Å, α = 90°, β = 90.322(1)°, γ = 90°; V = 3325.8(4) Å^3; d(calc) = 1.793 Mg/m^3; F(000) = 1776. Reflections (30 644) obtained over 1.44 ≤ 2θ ≤ 56.62 (98.4% completeness at maximum 2θ); max/min transmission coefficients, 0.6807/0.5209; μ(Mo Kα) = 2.084 mm^{-1}. Full-matrix least-squares refinement on 8169 independent merged (R(int) = 0.0342) reflections (269 parameters, 6 restraints) converged at $wR_2(F^2)$ = 0.0885 for all data; $R_1(F)$ = 0.0332 for $I > 2\sigma(I)$; GOF (on F^2) = 1.077; max/min residual electron density, 1.328 and −0.711 e·A^{-3}. The structure of **5a** consists of two independent *cis*-$PdCl_2(PMe_3)_2$ molecules together with two solvated $CHCl_3$ molecules. Methyl groups attached to the P1 atom are disordered over two sites with an occupancy factor of 0.65/0.35.

The crystal of **5a** was a pseudo-merohedral twin crystal with a ratio of domains of 0.88/0.12. Although the contribution from a second component was low (~10%), the twin law, [−100, 0−10, 001], used in least-squares refinement improved the R_1 value significantly from 0.083 (before twin modeling) to 0.033.

■ ASSOCIATED CONTENT

Supporting Information

Crystallographic information files (CIF) for the reported structures; Table S1 with the comparative mean distances and individual ranges for **1a**, **1b**, and **2a**; Figure S1 (contour maps of anisotropic deformation of electron density about the Au_4 core); energy considerations for Pd_4 and Au_4 kernels in **1** and **2**. This material is available free of charge via the Internet at http://pubs.acs.org. Crystallographic data (in CIF files) have been deposited with the Cambridge Crystallographic Data Centre, 12 Union Road, Cambridge CB2 IEZ, United Kingdom, and copies can be obtained upon request, free of charge, by quoting the publication citation and the CCDC deposition numbers 1040120 (**1a**), 1040122 (**1b**), and 1040121 (**5a**) via www.ccdc.cam.ac.uk/data_request/cif.

■ AUTHOR INFORMATION

Corresponding Authors

*E-mail: mednikov@chem.wisc.edu. (E.G.M)

*E-mail: dahl@chem.wisc.edu. (L.F.D.)

Notes

The authors declare no competing financial interest.

■ ACKNOWLEDGMENTS

This research was supported by the Univ. of Wisconsin-Madison and the Hilldale Foundation (UW-Madison). The SMART 1000 CCD X-ray area-detector system was purchased, in part, from National Science Foundation Grant No. CHE-9310428. Structural drawings were prepared with Crystal Maker Software (D. C. Palmer, Centre for Innovation & Enterprise, Begbroke Science Park, Bldg 5, Sandy Lane, Yarnton, Oxfordshire OX5 1PF, U.K.). We are grateful to Prof. John F. Berry (Chem. Dept.; UW-Madison) and Prof. June Dahl (Dept. of Neuroscience; UW School of Medicine & Public Health) for helpful comments. We also thank Dr. Ilia Guzei (Chem. Dept.; UW-Madison) for crystallographic advice and the use of the Departmental X-ray Crystallographic Facilities.

■ DEDICATION

We dedicate this paper to Professor Giuliano Longoni in honor of his recent retirement from the University of Bologna and in

DOI: 10.1021/acs.inorgchem.5b00208
Inorg. Chem. XXXX, XXX, XXX−XXX

recognition of his highly creative, inspirational leadership and the resulting major scientific impacts of the many important contributions that he and his co-workers have made to metal carbonyl cluster chemistry during the past 40 years.

REFERENCES

(1) Braye, E. H.; Dahl, L. F.; Hübel, W.; Wampler, D. L. *J. Am. Chem. Soc.* **1962**, *84*, 4633−4639.

(2) For reviews, see: (a) Zanello, P. *Phys. Organomet. Chem.* **2002**, *3* (*Unusual Structures and Physical Properties in Organometallic Chemistry*), 1. [Zanello, P. In *Unusual Structures and Physical Properties in Organometallic Chemistry;* Gielen, M., Willem, R., Wrackmeyer, B., Eds.; John Wiley & Sons Ltd.: New York, 2002; pp 1−49]. (b) Johnson, B. F. G.; Martin, C. M. In *Metal Clusters in Chemistry;* Braunstein, P., Oro, L. A., Raithby, P. R., Eds.; Wiley-VCH: New York, 1999; Vol. *2*, pp 877−912. (c) Dyson, P. J. *Adv. Organomet. Chem.* **1998**, *43*, 43−124. (d) Gubin, S. P. *Pure Appl. Chem.* **1986**, *58*, 567−574. (e) Bradley, J. S. *Adv. Organomet. Chem.* **1983**, *22*, 1−58. (f) Tachikawa, M.; Muetterties, E. L. *Prog. Inorg. Chem.* **1981**, *28*, 203−238.

(3) (a) Takemoto, S.; Matsuzaka, H. *Coord. Chem. Rev.* **2012**, *256*, 574−588. (b) Bernardi, A.; Ciabatti, I.; Femoni, C.; Iapalucci, M. C.; Longoni, G.; Zacchini, S. *Dalton Trans.* **2013**, *42*, 407−421. (c) Saha, S.; Zhu, L.; Captain, B. *Inorg. Chem.* **2013**, *52*, 2526−2532. (d) Randles, M. D.; Dewhurst, R. D.; Cifuentes, M. P.; Humphrey, M. G. *Organometallics* **2012**, *31*, 2582−2588. (e) Della Pergola, R.; Sironi, A.; Garlaschelli, L.; Strumolo, D.; Manassero, C.; Manassero, M.; Fedi, S.; Zanello, P.; Kaswalder, F.; Zacchini, S. *Inorg. Chim. Acta* **2010**, *363*, 586−594. (f) Nakajima, T.; Konomoto, H.; Ogawa, H.; Wakatsuki, Y. *J. Organomet. Chem.* **2007**, *692*, 5071−5080. (g) Chisholm, D. M.; McIndoe, J. S.; Bodizs, G.; Ang, W. H.; Scopelliti, R.; Dyson, P. J. *J. Cluster Sci.* **2007**, *18*, 303−318. (h) Koshevoy, I. O.; Haukka, M.; Pakkanen, T. A.; Tunik, S. P. *Dalton Trans.* **2006**, 5641−5647. (i) Mironov, Yu. V.; Naumov, N. G.; Kozlova, S. G.; Kim, S.-J.; Fedorov, V. E. *Angew. Chem.* **2005**, *117*, 7027−7031; *Angew. Chem., Int. Ed.* **2005**, *44*, 6867−6871. (j) Khimyak, T.; Johnson, B. F. G.; Hermans, S.; Bond, A. D. *Dalton Trans.* **2003**, 2651−2657. (k) Fumagalli, A.; Costa, M.; Della Pergola, R.; Zanello, P.; Fabrizi de Biani, F.; Macchi, P.; Sironi, A. *Inorg. Chim. Acta* **2003**, *350*, 187−192. (l) Lau, J. P.-K.; Wong, W.-T. *Inorg. Chem. Commun.* **2003**, *6*, 733−736. (m) Bruce, M. I.; Zaitseva, N. N.; Skelton, B. W.; White, A. H. *J. Chem. Soc., Dalton Trans.* **2002**, 3879−3885.

(4) (a) Chung, C.; Tseng, W.-C.; Chi, Y.; Peng, S.-M.; Lee, G.-H. *Organometallics* **1998**, *17*, 2207−2214. and references therein. (b) Chisholm, M. H.; Hammond, C. E.; Johnston, V. J.; Streib, W. E.; Huffman, J. C. *J. Am. Chem. Soc.* **1992**, *114*, 7056−7065. and references therein. (c) Dutton, T.; Johnson, B. F. G.; Lewis, J.; Owen, S. M.; Raithby, P. R. *J. Chem. Soc., Chem. Commun.* **1988**, 1423−1424. (d) Neithamer, D. R.; LaPointe, R. E.; Wheeler, R. A.; Richeson, D. S.; Van Duyne, G. D.; Wolczanski, P. T. *J. Am. Chem. Soc.* **1989**, *111*, 9056−9072. (e) Bradley, J. S.; Ansell, G. B.; Leonowicz, M. E.; Hill, E. W. *J. Am. Chem. Soc.* **1981**, *103*, 4968−4970. (f) Wijeyesekera, S. D.; Hoffmann, R.; Wllker, C. N. *Organometallics* **1984**, *3*, 962−970. (g) Bogdan, P. L.; Woodcock, C.; Shriver, D. F. *Organometallics* **1987**, *6*, 1377−1381. (h) Tachikawa, M.; Muetterties, E. L. *J. Am. Chem. Soc.* **1980**, *102*, 4541−4542. For review, see: (i) Shriver, D. F.; Sailor, M. J. *Acc. Chem. Res.* **1988**, *21*, 374−379 and references therein.

(5) (a) Goodman, D. W. *Annu. Rev. Phys. Chem.* **1986**, *37*, 425−457. (b) Keim, W. *In Catalysis in C_1 Chemistry;* Keim, W., Ed.; D. Reidel Publ. Comp.: Dordrecht, the Netherlands, 1983; pp 5−39, and references therein. (c) Röper, M. ibid.; pp 41−88, and references therein.

(6) (a) Roscher, G. Vinyl Esters. In *Ullmans' s Encyclopedia of Industrial Chemistry;* Elvers, B., Hawkins, S., Eds.; Federal Republic of Germany: VCH Verlagsgesellschaft: Weinheim, Germany, 1996; Vol. *A27*, p 423 (pp 419−434). (b) Provine, W. D.; Mills, P. L.; Lerou, J. J. in *11th International Congress on Catalysis − 40th Anniversary*, Hightower, J. W., Delgass, W. N., Iglesia, E., Bell, A. T., Eds.; *Stud. Surf. Sci. Catal.*, **1996**, *101*, 191−200. (c) Neurock, M. *J. Catal.* **2003**, *216*, 73−88. (d) Bowker, M.; Morgan, C. *Catal. Lett.* **2004**, *98*, 67. (e) Han, Y.-F.; Kumar, D.; Sivadinarayana, C.; Clearfield, A.; Goodman, D. W. *Catal. Lett.* **2004**, *94*, 131−134. (f) Chen, M.; Kumar, D.; Yi, C.-W.; Goodman, D. W. *Science* **2005**, *310*, 291−293.

(7) (a) Mednikov, E. G.; Dahl, L. F. D. *J. Cluster. Sci.* **2005**, *16*, 287−302. (b) Mednikov, E. G.; Jewell, M. C.; Dahl, L. F. D. *J. Am. Chem. Soc.* **2007**, *129*, 11619−11630.

(8) Tran, N. T.; Kawano, M.; Dahl, L. F. *J. Chem. Soc., Dalton Trans.* **2001**, 2731−2748.

(9) (a) It was unambiguously shown from $^{31}P\{^1H\}$ NMR measurements that $Pd_xPt_y(CO)_5(PEt_3)_4$, $x + y = 4$, clusters were formed upon combined dissolution of $Pd_4(CO)_5(PEt_3)_4$ and $Pt_4(CO)_5(PEt_3)_4$ under N_2.[9b]. (b) Mednikov, E. G.; Dahl, L. F., unpublished research.

(10) Mednikov, E. G. *Metalloorgan. Khim.* **1991**, *4*, 1237−1240; *Organomet. Chem. in the USSR (Engl. Transl.)* **1991**, *4*, 608−610.

(11) Bochmann, M.; Hawkins, I.; Hursthouse, M. B.; Short, R. L. *Polyhedron* **1987**, *6*, 1987−1991.

(12) Albano, V. G.; Sansoni, M.; Chini, P.; Martinengo, S. *J. Chem. Soc., Dalton Trans.* **1973**, 651−655.

(13) Calderoni, F.; Demartin, F.; Fabrizi de Biani, F.; Femoni, C.; Iapalucci, M. C.; Longoni, G.; Zanello, P. *Eur. J. Inorg. Chem.* **1999**, 663−671.

(14) Burrows, A. D.; Mingos, D. M. P.; Menzer, S.; Vilar, R.; Williams, D. J. *J. Chem. Soc., Dalton Trans.* **1995**, 2107−2108.

(15) (a) Gracia, J.; Martín, A.; Mena, M.; Morales-Varela, M. C.; Poblet, J.-M.; Santamaría, C. *Angew. Chem.* **2003**, *115*, 957−960; *Angew. Chem., Int. Ed.* **2003**, *42*, 927−930. (b) Jeffery, J. C.; Parrot, M. J.; Stone, F. G. A. *J. Organomet. Chem.* **1990**, *382*, 225−235. (c) Farrugia, L. J.; Miles, A. D.; Stone, F. G. A. *J. Chem. Soc., Dalton Trans.* **1985**, 2437−2447. (d) Hriljac, J. A.; Harris, S.; Shriver, D. F. *Inorg. Chem.* **1988**, *27*, 816−821.

(16) Zhao, Y.; Truhlar, D. G. *J. Chem. Phys.* **2006**, *125*, 194101−194118.

(17) Frisch, M. J.; Trucks, G. W.; Schlegel, H. B.; Scuseria, G. E.; Robb, M. A.; Cheeseman, J. R.; Scalmani, G.; Barone, V.; Mennucci, B.; Petersson, G. A.; Nakatsuji, H.; Caricato, M.; Li, X.; Hratchian, H. P.; Izmaylov, A. F.; Bloino, J.; Zheng, G.; Sonnenberg, J. L.; Hada, M.; Ehara, M.; Toyota, K.; Fukuda, R.; Hasegawa, J.; Ishida, M.; Nakajima, T.; Honda, Y.; Kitao, O.; Nakai, H.; Vreven, T.; Montgomery, J. A., Jr.; Peralta, J. E.; Ogliaro, F.; Bearpark, M.; Heyd, J. J.; Brothers, E.; Kudin, K. N.; Staroverov, V. N.; Kobayashi, R.; Normand, J.; Raghavachari, K.; Rendell, A.; Burant, J. C.; Iyengar, S. S.; Tomasi, J.; Cossi, M.; Rega, N.; Millam, M. J.; Klene, M.; Knox, J. E.; Cross, J. B.; Bakken, V.; Adamo, C.; Jaramillo, J.; Gomperts, R.; Stratmann, R. E.; Yazyev, O.; Austin, A. J.; Cammi, R.; Pomelli, C.; Ochterski, J. W.; Martin, R. L.; Morokuma, K.; Zakrzewski, V. G.; Voth, G. A.; Salvador, P.; Dannenberg, J. J.; Dapprich, S.; Daniels, A. D.; Farkas, Ö.; Foresman, J. B.; Ortiz, J. V.; Cioslowski, J.; Fox, D. J. *Gaussian 09,* Revision B.01; Gaussian, Inc.: Wallingford, CT, 2009.

(18) Hay, P. J.; Wadt, W. R. *J. Chem. Phys.* **1985**, *82*, 299−310.

(19) Check, C. E.; Faust, T. O.; Bailey, J. M.; Wright, B. J.; Gilbert, T. M.; Sunderlin, L. S. *J. Phys. Chem. A* **2001**, *105*, 8111.

(20) (a) Kohn, W.; Sham, L. J. *Phys. Rev.* **1965**, *140*, A1133−A1138. (b) Vosko, S. H.; Wilk, L.; Nusair, M. *Can. J. Phys.* **1980**, *588*, 1200−1211.

(21) Wiberg, K. B. *Tetrahedron* **1968**, *24*, 1083−1096.

(22) Hakkinen, H.; Landman, U. *Phys. Rev. B* **2000**, *62* (4), R2287−R2290.

(23) Mednikov, E. G.; Ivanov, S. A.; Dahl, L. F. *Inorg. Chem.* **2011**, *50*, 11795−11806.

(24) (a) Hui, J. W.-S.; Wong, W.-T. *J. Cluster Sci.* **1999**, *10*, 91−108. (b) Hui, J. W.-S.; Wong, W.-T. *J. Chem. Soc., Dalton Trans.* **1996**, 2887−2888. (c) Gubin, S. P.; Galuzina, T. V.; Golovaneva, I. F.; Klyagina, A.P.; Polyakova, L. A.; Belyakova, O. A.; Zubavichus, Ya. V.; Slovokhotov, Yu. L. *J. Organomet. Chem.* **1997**, *549*, 55−72. (d) Gubin, S. P.; Klyagina, A. P.; Golovaneva, I. F.; Galuzina, T. V.; Belyakova, O. A.; Zubavichus, Ya. V.; Slovokhotov, Yu. L. *Inorg. Chim. Acta* **1998**,

DOI: 10.1021/acs.inorgchem.5b00208
Inorg. Chem. XXXX, XXX, XXX−XXX

280, 275−281. (e) Nakajima, T.; Ishiguro, A.; Wakatsuki, Y. *Angew. Chem.* **2000**, *112*, 1175−1177; *Angew. Chem., Int. Ed.* **2000**, *39*, 1131−1134. (f) Adams, R. D.; Captain, B.; Fu, W.; Pellechia, P. J.; Smith, M. D. *Inorg. Chem.* **2003**, *42*, 2094−2101. (g) Hui, J. W.-S.; Wong, W.-T. *J. Chem. Soc., Dalton Trans.* **1997**, 2445−2450. (h) Hui, J. W.-S.; Wong, W.-T. *J. Chem. Soc., Dalton Trans.* **1998**, 2065−2070. (i) Polyakova, L. A.; Churakov, A. V.; Kuz'mina, L. G.; Golovaneva, I. F.; Klyagina, A. P.; Gubin, S. P. *Zh. Neorg. Khim.* **2003**, *48*, 1110−1116; *Russ. J. Inorg. Chem. (Engl. Transl.)* **2003**, *48*, 1001−1007. (j) Ciabatti, I.; Femoni, C.; Gaboardi, M.; Iapalucci, M. C.; Longoni, G.; Pontiroli, D.; Ricco, M.; Zacchini, S. *Dalton Trans.* **2014**, *43*, 4388−4399. (k) Ciabatti, I.; de Biani, F. F.; Femoni, C.; Iapalucci, M. C.; Longoni, G.; Zacchini, S. *ChemPlusChem* **2013**, *78*, 1456−1465.

(25) Allen, F. H. *Acta Crystallogr., Sect. B: Struct. Sci.* **2002**, *58*, 380−388.

(26) (a) Grdenič, D.; Korpar-Čolig, B.; Matkovič-Čalogovič, D. *J. Organomet. Chem.* **1996**, *522*, 297−302. and references therein. (b) Grdenič, D.; Kamenar, B.; Korpar-Čolig, B.; Sikirica, M.; Jovanovski, G. *Cryst. Struct. Commun.* **1982**, *11*, 565−568. and references therein. (c) Kroon, J.; Hulscher, J. B.; Peerdeman, A. F. *J. Organomet. Chem.* **1970**, *23*, 477−485. (d) Klinkhammer, K. W.; Kuhner, S.; Regelmann, B.; Weidlein, J. *J. Organomet. Chem.* **1995**, *496*, 241−243. (e) Matsunaga, P. T.; Kouvetakis, J.; Groy, T. L. *Inorg. Chem.* **1995**, *34*, 5103−5104. (f) Although we included two $Au_4(\mu_4$-C) clusters, the reported $(\mu_4$-C)$[AuP(o\text{-}MeC_6H_4)_3]_4$ and $(\mu_4$-C)$[AuP(C_6H_{11})_3]_4$ were not crystallographically characterized: Schmidbaur, H.; Steigelmann, O. *Z. Naturforsch., B* **1992**, *47*, 1721−1724. (g) Graham, T. D.; Ong, C.; Wei, P.; Stephan, D. W. *J. Organomet. Chem.* **2007**, *692*, 4481−4485. and references therein. (h) Ong, C.; Kickham, J.; Clemens, S.; Guerin, F.; Stephan, D. W. *Organometallics* **2002**, *21*, 1646−1653. and references therein. (i) Kickham, J. E.; Guérin, F.; Stephan, D. W. *J. Am. Chem. Soc.* **2002**, *124*, 11486−11494.

(27) Gong, J.-H.; Tsay, C.-W.; Tu, W.-C.; Chi, Y.; Peng, S.-M.; Lee, G.-H. *J. Cluster Sci.* **1995**, *6*, 289−309.

(28) Takahashi, Y.; Akita, M.; Moro-oka, Y. *Chem. Commun.* **1997**, 1557−1558.

(29) (a) Davies, D. L.; Jeffery, J. C.; Miguel, D.; Sherwood, P.; Stone, F. G. A. *J. Chem. Soc., Chem. Commun.* **1987**, 454−456. (b) Davies, D. L.; Jeffery, J. C.; Miguel, D.; Sherwood, P.; Stone, F. G. A. *J. Organomet. Chem.* **1990**, *383*, 463−480.

(30) Franolic, J. D.; Long, J. R.; Holm, R. H. *J. Am. Chem. Soc.* **1995**, *117*, 8139−8153 and references therein.

(31) Beringhelli, T.; Ciani, G.; D'Alfonso, G.; Sironi, A.; Freni, M. *J. Chem. Soc., Chem. Commun.* **1985**, 978−979.

(32) Mednikov, E. G.; Tran, N. T.; Aschbrenner, N. L.; Dahl, L. F. *J. Cluster Sci.* **2007**, *18*, 253−269.

(33) Mednikov, E. G.; Eremenko, N. K. *Izv. Akad. Nauk, Ser. Khim.* **1982**, 2540−2545; *Bull. Acad. Sci. USSR, Div. Chem. Sci.* **1982**, *31*, 2240−2245 (Engl. Transl.).

(34) Schultz, G.; Subbotina, N. Yu.; Jensen, C. M.; Golen, J. A.; Hargittai, I. *Inorg. Chim. Acta* **1992**, *191*, 85−90.

(35) Sheldrick, G. All crystallographic software and sources of the scattering factors are contained in the program library of *SHELXL-97;* Bruker Analytical X-Ray Systems: Madison, WI, 2015.

DOI: 10.1021/acs.inorgchem.5b00208
Inorg. Chem. XXXX, XXX, XXX−XXX